Applied Catalysis B: Environmental 206 (2017) 328–335

Contents lists available at ScienceDirect

Applied Catalysis B: Environmental

journal homepage: www.elsevier.com/locate/apcatb

In-situ synthesis of Cu nanoparticles hybridized with carbon quantum dots as a broad spectrum photocatalyst for improvement of photocatalytic H_2 evolution

Piyong Zhang, Ting Song, Tingting Wang, Heping Zeng*

Key Laboratory of Functional Molecular Engineering of Guangdong Province, School of Chemistry and Chemical Engineering, South China University of Technology, Guangzhou, 510641, PR China

ARTICLE INFO

Article history:
Received 26 November 2016
Received in revised form 9 January 2017
Accepted 20 January 2017
Available online 22 January 2017

Keywords:
Plasmonic Cu/CQDs photocatalyst
Broad spectrum activity
Hydrogen evolution

ABSTRACT

Exploration of broad spectrum photocatalyst for photocatalytic reaction is of great importance. Cu nanoparticles (NPs) were used for photocatalytic hydrogen evolution due to its surface plasmon resonance (SPR) effect and broad spectrum response. Here, Cu NPs were modified with carbon quantum dots (CQDs) for further improvement of photocatalytic ability. Cu/CQDs composites were prepared by facile *in-situ* photoreduction and a much higher H_2 evolution rate was achieved than that of pure Cu NPs. The highest H_2 evolution rate was 64 mmol g^{-1} h^{-1} for sample **C** which contains 15.6 wt% of CQDs. CQDs act as an electron reservoir to trap electrons generated from Cu NPs and hinder the recombination of electron-hole pair. Due to surface plasmon resonance (SPR) effect of Cu nanoparticles, broad spectrum photocatalytic activities of these samples were achieved under monochromatic light irradiation at 700, 800 and 900 nm, respectively. A possible mechanism is illustrated for the photocatalytic activity improvement of Cu nanoparticles modified with CQDs.

1. Introduction

Evolution of hydrogen with solar energy from water has attracted considerable attention due to environmental pollution and energy crisis [1]. Plasmonic metal nanoparticles (Au, Ag, Cu, etc.) are known to possess catalytic activities for efficient conversion of solar energy to chemical energy through surface plasmon resonance (SPR) effect [2–5]. SPR is induced by strong interaction of resonant photons and plasmonic metal nanoparticles (NPs) when their frequencies are identical. Metal SPR is of a lower energy than the semiconductor band gap which allows for a broad absorption band and it has been applied to plasmonic metal photocatalysts [6–11]. Plasmonic Cu NPs have attracted much attention due to its low cost, high conductivity, near-infrared response (800 ~ 900 nm) and promising photocatalytic activity [3,9–13]. Hence, a feasible process to obtain Cu NPs should be considered for hydrogen evolution.

Recently, carbon quantum dots (CQDs) have attracted tremendous interest among researchers because of their special properties, including good chemical stability [14], abundant, inexpensive, ease of bio-conjugation [15], photo-induced charge transfer property and excellent up-conversion luminescence properties [16]. CQDs can act as a multifunctional component in the design of photocatalyst to enhance the separation of electron-hole pair. In the reported photocatalytic systems, the substrate materials modified with CQDs are semiconductors, such as Bi_2SiO_5 [17], WO_3 [18], g-C_3N_4 [19,20], Bi_2WO_6 [21] and TiO_2 [22–24]. To the best of our knowledge, there is no report on CQDs modified plasmonic Cu NPs in the photocatalytic hydrogen evolution.

Based on our researches [9,25–29], we reported a convenient *in-situ* method for the generation of Cu NPs under vacuum conditions and here, they were modified with CQDs further. Photocatalytic hydrogen evolution of Cu/CQDs composite was evaluated using lactic acid solution as a sacrificial agent under solar light irradiation. Under monochromatic light irradiation at wavelengths of 700, 800 and 900 nm, Cu NPs and Cu/CQDs still exhibit good photocatalytic activities. This is an important exploration in near-infrared light utilization.

* Corresponding author.
E-mail address: hpzeng@scut.edu.cn (H. Zeng).

http://dx.doi.org/10.1016/j.apcatb.2017.01.051
0926-3373/

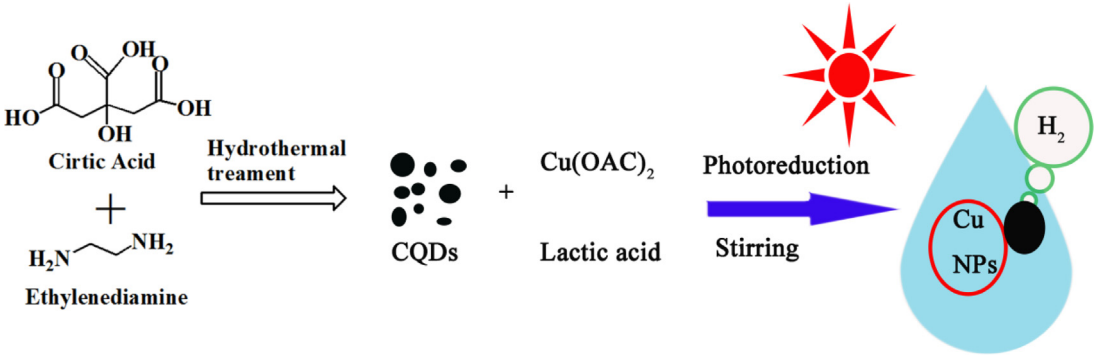

Scheme 1. Illustration of the synthesis procedure for Cu/CQDs.

2. Experimental

2.1. Materials

All reagents were analytical grade and used without further purification. Deionized water was used in all experiments. Copper acetate hydrate ($Cu(CH_3COO)_2{\cdot}H_2O$ AR), lactic acid (97%), polyethylene glycol (M_w = 2000), ethylenediamine (AR), terephthalic acid and citri acid (AR) were purchased from Sinopharm Chemical Reagent Co. Ltd., P.R. China.

2.2. Synthesis of CQDs

CQDs were prepared as follows: ethylenediamine (0.2 mL) and citric acid (0.21 g) were dissolved in deionized water (5 mL), and stirred to form a clear solution. Then the solution was transferred to a Teflon autoclave (15 mL), followed by a heat at 180 °C for 5 h. After natural cooling to room temperature, the brown-black and transparent solution was sonicated for 60 min. The purification step (to remove residual ethylenediamine and citric acid) of the supernatant was processed by dialysis (1 kDa, MWCO) for approximately 24 h in the flowing water to achieve high purity CQDs. At last, the CQDs were isolated by freeze-drying and they are yellow-orange powder. In addition, 5 mg of CQDs was dissolved in 50 mL of volumetric flask to obtain 0.1 g L^{-1} CQDs solution which was diluted to a final concentration of 0.01 g L^{-1}.

2.3. Characterization

X-ray diffraction (XRD) patterns were performed on a D8 X-ray diffractometer (German, Bruker AXS) using Cu-Kα radiation. Transmission electron microscopy (TEM) images were taken on a JEOL JEM-2100 electron microscope equipped with energy dispersive X-ray (EDX) spectrometer. X-ray photoelectron spectroscopy (XPS) data were obtained on a Kratos Axis-Ultra DLD (equipped with AES) instrument with a monochromatized Al-Kα line source (150 W). Scanning electron microscopy (SEM) images was obtained with a Zeiss Merlin (Germany, Zeiss Co.) emission scanning electron microscope. Fourier transform infrared (FT-IR) spectra were recorded using a FT-IR spectrometer (Nicolet 670) for samples dispersed in KBr pellets in 1:99 ratios. The analysis of photoluminescence spectra (PL) was carried out at room temperature on a Hitachi F-4500 fluorescence spectrophotometer. Fluorescence lifetime were collected on an (Edinburge Instruments, England) FLS 980 spectrometer. The UV–vis diffuse reflection absorption spectra were obtained by a UV–vis spectrometer (Japan, Hitachi, U3010, referenced by $BaSO_4$) equipped with an integrating sphere accessory in the diffuse reflectance mode. Raman spectra were obtained by Laser Confocal Raman Microscopy system (LabRAM Aramis, H.J.Y, France).

2.4. Photocatalytic hydrogen evolution

The photocatalytic experiments were performed in a 300 mL Pyrex reaction cell which connected to an evacuation system and closed gas circulation. A 300 W Xe lamp (PLS-SXE300CUV, Perfect light. Co. Ltd., Beijing) was used in photocatalytic experimental. Based on our previous research [9], 1 mL of 2 mmol L^{-1} copper acetate solution was taken as the precursor in *in-situ* synthesis process. Information of samples is shown in table S1 and the schematic of synthesis procedure for samples is described in Scheme 1. Theoretical content of CQDs in Cu/CQDs samples are 0 wt%, 7.8 wt%, 15.6 wt%, 23.4 wt%, 31.2 wt%, 39 wt% for samples **A–F**, respectively. The total volume of reaction solution is 70 mL and the temperature of the reaction was kept at 278 K by cool flowing water. The aqueous solution was completely degassed about 0.5 h and then irradiated by a xenon lamp without any filter. After irradiation, Cu NPs were generated and the combination between Cu NPs and CQDs was taken place at the same time. Meanwhile, photocatalytic H_2 evolution was carried out. Hydrogen evolution was analyzed by online gas chromatography (Tian mei, GC-7900, 5 Å molecular sieve column, nitrogen as a carrier gas) with a thermal conductivity detector (TCD). Photocatalytic experiments of samples **A–F** were also carried out under visible light irradiation with a UV cut off filter (λ > 420 nm).

Samples **A** and **C** were selected to carry out long-wavelength photocatalytic experiment. 700, 800, 900 nm wavelength band pass filters were installed on xenon lamp and other experimental conditions remain unchanged. Bandwidth of band pass filters were 700 ± 10, 800 ± 10, and 900 ± 10 nm. Samples were harvested by centrifugation at 10,000 rpm for 20 min after hydrogen evolution reaction and the whole processes were carried out under nitrogen protection.

Photocatalytic hydrogen evolution experiments of physical mixture of Cu and CQDs were also performed. 1 mL of 2 mmol L^{-1} copper acetate solution, 10 mL of lactic acid, 56 mL deionized water and 1 g PEG were added in Pyrex reaction cell. The aqueous solution was completely degassed about 0.5 h and then irradiated by a xenon lamp without any filter. After 5 h irradiation, 2 mL of 0.01 g L^{-1} CQDs solution was added in the reaction solution and continuing to irradiate. Cu NPs were generated firstly and then CQDs were added in the solution. Although the composition in the solution is same as sample **C**, Cu and CQDs were physical mixture in the solution. Hydrogen evolution rate was analyzed by online gas chromatography every hour.

2.5. Photoelectrochemical measurements

Electrochemical measurements of Cu NPs and Cu/CQDs were conducted in a conventional three electrode cell by electrochemical analyzer (CHI660C Instruments, Shanghai, China). Cu NPs

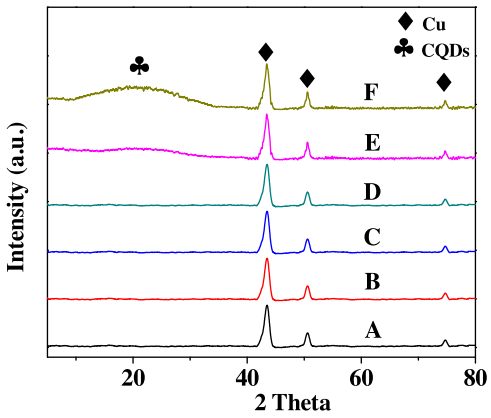

Fig. 1. XRD patterns of samples **A–F**.

and Cu/CQDs electrodes served as the working electrode, using a platinum wire as the counter electrode and a saturated Ag/AgCl electrode as the reference electrode. 0.1 M Na_2SO_4 aqueous solution was used as electrolyte without additive for the photocurrent measurement. The preparation of working electrode was shown as follows: ITO electrode was placed in the solution which has the same composition with Table 1 and irradiated with 300 W Xenon arc lamp about 1 h. Then the ITO electrode was taken out and washed with deionized water and ethanol three times, respectively. After washing, the electrode was dried at 323 K for 3 h under vacuum condition. The whole process is under protection of positive N_2 pressure. A 300 W Xenon arc lamp was employed as the light source for the photocurrent measurement.

2.6. Measurement of •OH radicals generated from the oxidation by photogenerated holes

The •OH radical reactions were performed as follows: 10 mg of samples **A–F** were suspended in a 10 mL solution containing 10 mM of NaOH and 5 mM of terephthalic acid, respectively. The suspension was first stirred in dark for 10 min. After 10-min solar light irradiation, the suspension was centrifuged. The upper clear solution was then taken for measuring the fluorescence of 2-hydroxyterephthalic acid using a spectrofluorometer (Hitachi F-4500) with an excitation wavelength of 320 nm.

3. Results and discussion

3.1. Formation and characterization

The phase structures of the prepared samples were investigated by X-ray diffractometer and the results are shown in Fig. 1. The diffraction peaks appearing at 43.3°, 50.5°, and 74.1° correspond to the (111), (200) and (220) planes, respectively, which are attributed to face centered cubic copper (JCPDS No. 04-0836) [9]. The broad diffraction peaks which present in samples **E** and **F** at 21.4° match well with (002) plane of CQDs [30]. The peak of CQDs is wider than Cu due to its poor crystalline and micro size. Characteristic peak of CQDs cannot be detected in samples **B–D**, which may be ascribed to poor crystalline and low CQDs content in the samples [16,31]. In addition, XRD pattern of pure CQDs is supplied in Fig. S1 and it has a significant characteristic peak at 21.4°. XRD patterns of Cu/CQDs composites reveal a coexistence Cu and CQDs, and possible impurities (CuO and Cu_2O) are not detected by XRD, indicating the high purity of samples. Moreover, crystalline form of Cu didn't change after combination with CQDs suggesting that there is no doping in the face centered cubic copper.

Fig. 2a shows UV–vis diffuse reflectance spectra of samples **A–F** and CQDs. The absorption peak about 230 nm of CQDs is typically assigned to the π-π* transition from the carbon core [32], similar to polycyclic aromatic hydrocarbons [33]. Absorption peak at 362 nm is attributed to the surface section and contribution of the n-π* transition [32,34]. For sample **A** (pure Cu NPs), absorption band from 200 to 900 nm is ascribed to surface plasmon resonance band of Cu NPs and a characteristic absorption peak at 600 nm is observed for plasmonic Cu NPs [3,9]. Due to the absorption band of Cu NPs, a large fraction of the abundant solar flux consists of UV–vis and near-infrared photons can be utilized for the photocatalytic reaction. After combination with CQDs, intensity of absorption band decreases with the increasing content of CQDs for simples **B–F** due to their poor response in visible light region. However, a significant enhancement of absorption is observed at 362 nm because of contribution of CQDs. This could also illustrate that Cu NPs modify with CQDs successfully.

The Raman spectra of Cu/CQDs and CQDs are shown in Fig. 2b. According to reference [35], the representative bands of CQDs are located at 1611 and 1343 cm^{-1} assigned to G-band and D-band of carbon respectively. There is no band for Cu NPs because it has no responding in Raman spectra. Compared with pure CQDs, the intensity of D-band and G-band of Cu/CQDs is enhanced due to surface-enhanced Raman scattering (SERS) effect of Cu NPs with appropriate shape and size [3]. SERS signal enhancement indicates charge transfer between metal NPs and the molecule happens due to excitations [36]. Because of efficient charge transfer, more pho-

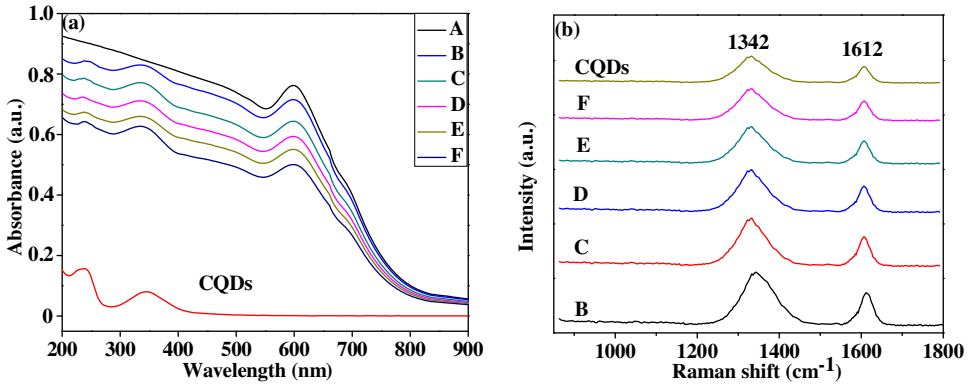

Fig. 2. (a) UV–vis diffuse reflectance spectra of samples **A–F** and CQDs, (b) Raman spectra of pure CQDs and samples **B–F**.

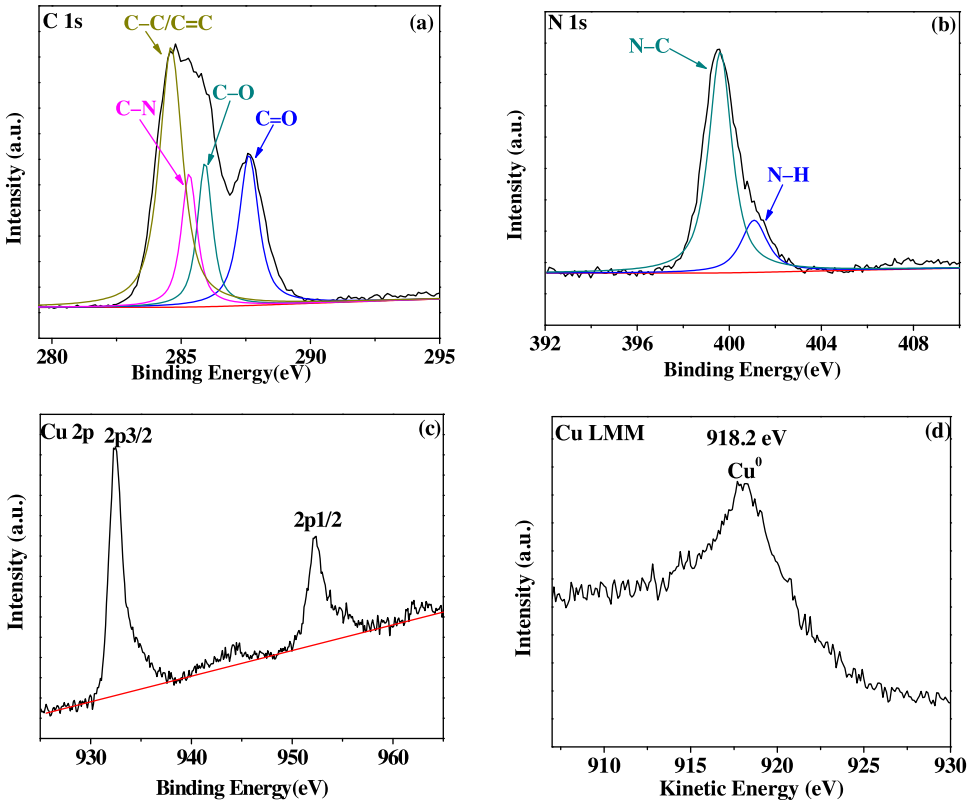

Fig. 3. XPS spectra of sample **C**: (a) C1s, (b) N1s, (c) Cu2p and (d) Cu LMM.

togenerated electrons will participate in photocatalytic reaction rather than combination with holes.

FTIR spectra of Cu/CQDs (sample **C**) were also investigated and the results are shown in Fig. S2. To further determine the surface composition and chemical state of Cu/CQDs, sample **C** was characterized by XPS and the results are shown in Fig. 3. The binding energies which obtained in the XPS analysis were corrected by referencing C 1s to 284.6 eV with specimen charging. Survey spectrum (Fig. S3) shows the presence of C, N, O and Cu in the sample. The C1s spectrum (Fig. 3a) can be fitted into four distinct carbon states at 284.6, 285.5, 286.2 and 288.2 eV, corresponding to various carbon C—C/C=C, C—N, C—O and C=O [37,38]. The XPS spectrum of N1s (Fig. 3b) exhibits two fitted peaks at 399.8 and 401.2 eV, which are assigned to N—C and N—H groups, respectively [29]. The curve fitting of O 1s spectrum (Fig. S4) reveals two peaks at 532.3 and 531.1 eV, which are associated with the C—OH/C—O—C and C=O bands, respectively [38]. Characteristic peaks of the Cu2p spectrum (Fig. 3c) at 932.5 and 952.7 eV are observed and attributed to the binding energy of Cu2p3/2 and Cu2p1/2, respectively. The results suggest that the high valence state Cu^{2+} species are effectively reduced to Cu^{+} or/and Cu^{0} because the characteristic satellite peaks of Cu^{2+} species at about 11 eV higher than 932.5 eV (Cu $2p_{3/2}$) have disappeared. Considering that the Cu^{+} and Cu^{0} have almost the same binding energy of Cu $2p_{3/2}$, Cu LMM XAES is traditionally used to distinguish these two valence states by different kinetic energy [39,40]. According to Fig. 3d, the peak at 918.2 eV is attributed to Cu^{0}, indicating that sample **C** contains Cu rather than Cu_2O which is consistent with the results of XRD.

Morphologies and microstructures of the samples were elucidated by scanning electron microscopy (SEM), transmission electron microscope (TEM) and high-resolution transmission electron microscope (HRTEM). As shown in SEM images of Fig. 4a and b, Cu/CQDS particles are distributed evenly with 0.01 and 0.02 mg CQDs for samples **B** and **C**, respectively. As the content of CQDs increase gradually, agglomeration bulk appears in the image. The higher the content of CQDs is, the bigger particles obtain. From Fig. 4c–e, particles become bigger and bigger with 0.03, 0.04 and 0.05 mg CQDs for samples **D**–**F**, indicating that condition of agglomeration is more and more serious. Agglomeration will cause low charge transfer efficiency which have a negative effect for photocatalytic reaction [35]. From EDX spectrum (Fig. 4f) and elemental mapping patterns results (Fig. 4g), we can see existence of Cu, C, O and N. The black points in the TEM image of Fig. 4h are attributed to Cu/CQDs with a TEM image. HRTEM image (Fig. 4i) presents (111) plane of Cu and (200) plane of CQDs that have inherent spacing distance of 0.21 and 0.32 nm, respectively [9,41]. A panoramic view (Fig. 4j) with a size distribution in the inset shows that spherical nanoparticles are distributed evenly with an average particle size of 5.2 ± 1.1 nm. Particle size of Cu/CQDs NPs mainly distributes at 4–6 nm, showing that the preparation method of samples used in experiment is effective with a relatively narrow size distribution, since uniform particle size distribution is critical in the photocatalytic reaction system.

3.2. Photocatalytic hydrogen evolution

Before the actual photocatalytic experiments were performed, control experiments were carried out using a pure lactic acid (LA) solution in the absence of either copper acetate solution or irradiation. No H_2 was produced until the presence of copper acetate and LA solution under irradiation, indicating that H_2 is produced from a photocatalytic reaction by the *in-situ* formed Cu NPs in the LA solution. In addition, pure CQDs in the LA solution also could not produce hydrogen under irradiation. The average rates of hydrogen evolution within 5 h for Cu/CQDs are presented in Fig. 5a. Pure Cu NPs (simple **A**) reveals a relatively low H_2 evolution rate ($32\ mmol\ g^{-1}\ h^{-1}$) which agrees with reference [9]. After modification with CQDs, H_2 evolution rates of all the samples are higher

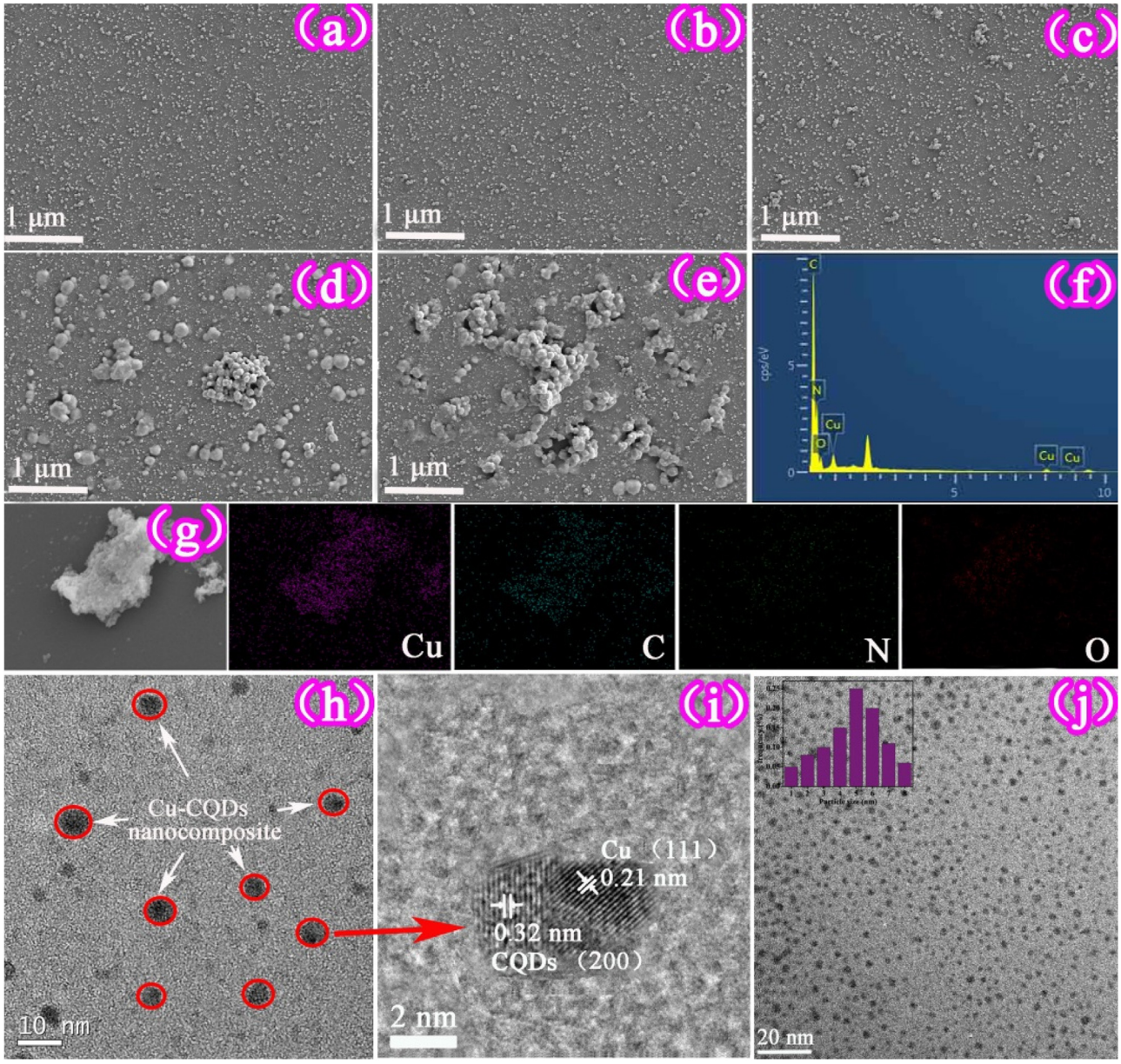

Fig. 4. SEM images (a) sample **B**, (b) sample **C**, (c) sample **D**, (d) sample **E**, (e) sample **F**; (f) EDX spectrum, (g) elemental mapping patterns, (h) TEM, (i) HRTEM, (j) TEM and size distribution (inset) images of sample **C** (Cu-CQDs nanocomposite).

than that of pure Cu NPs. From samples **A–C**, photocatalytic H_2 evolution rates increases stepwise. However, H_2 evolution rates of samples **D–F** which compared with sample **C** show slow decrease with the further increasing content of CQDs. The maximum hydrogen evolution rate is 64 mmol g^{-1} h^{-1} for sample **C** which is twice the rate of sample **A** (pure Cu NPs). This result suggests that appropriate content of CQDs could increase photocatalytic reaction rate because of an efficient interface between two components. On the contrary, too many CQDs would reduce photocatalytic ability due to formation of agglomerating state shown in Fig. 4 which becomes recombination centers of electron-hole [42–45]. In addition, photocatalytic H_2 evolution of samples **A–F** were performed under visible light irradiation ($\lambda > 420$ nm) and results are shown in Fig. S5.

The repeatability of sample **C** was tested in six consecutive runs of accumulatively 30 h under the same conditions as shown in Fig. 5b. It exhibits remarkable stability and little deactivation of the catalyst occurs upon repeated use. Furthermore, no great change was examined in surface element composition (Table S2) and XRD patterns (Fig. S6) before and after repeatability test, indicating that sample **C** has good stability during photocatalytic H_2 evolution. Moreover, chemical state of Cu was determined by XPS and comparison spectra of before and after recycle test are shown in Fig. S7. Both Cu2p spectrum (Fig. S7a) and Cu LMM (Fig. S7b) spectrum show inherent peaks and no impurities peaks are observed, suggesting sample **C** is stable in long time photocatalytic reaction.

Long-wavelength photocatalytic experiments of samples **A** (pure Cu NPs) and **C** were carried out with monochromatic light irradiation (700, 800, and 900 nm wavelength). As shown in Fig. 5c, photocatalytic H_2 evolution rate has a significant decrease under long-wavelength light irradiation due to the decrease of light energy import. From 700–900 nm wavelength, phocatalytic abilities of both Cu NPs and sample **C** are weakened gradually. Compared with most catalysts [15–20], however, they still keep some responses for photocatalytic reaction in near-infrared region due to the SPR effect of Cu NPs, which is meaningful to explore long-wavelength light catalytic reaction. In addition, photocatalytic H_2

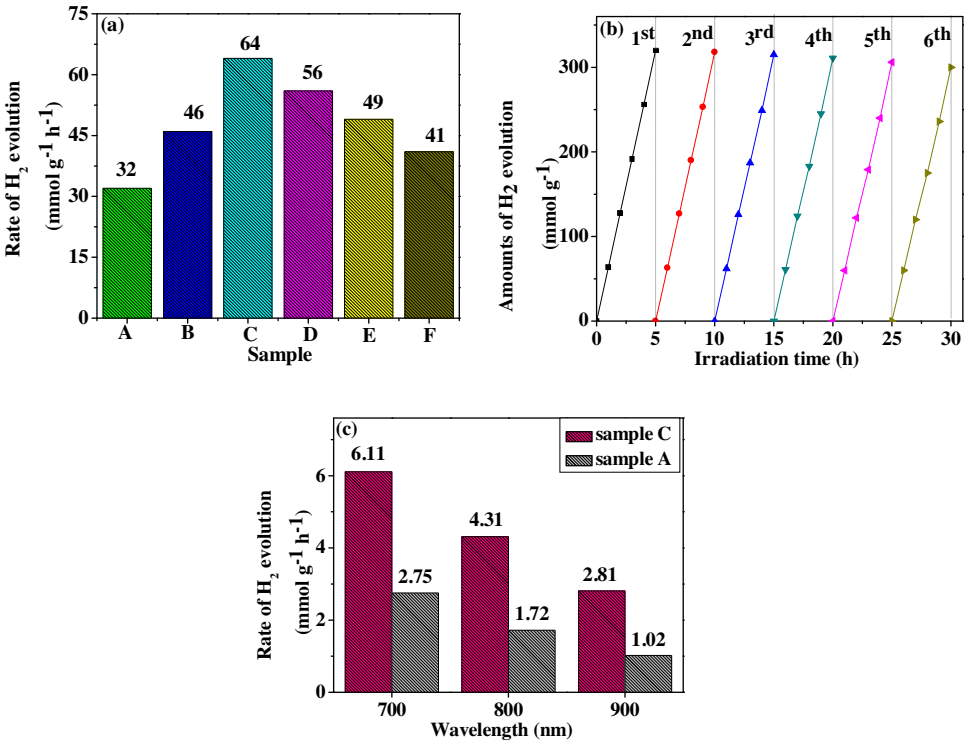

Fig. 5. (a) Photocatalytic H_2 evolution of samples **A**–**F** under solar light irradiation, (b) cycling test of photocatalytic H_2 evolution for sample **C** (irradiation time = 30 h), (c) photocatalytic H_2 evolution of samples **A** and **C** with monochromatic light irradiation.

evolution rate of sample **C** is higher than Cu NPs under different monochromatic light irradiation, suggesting that enhancement of phocatalytic ability with CQDs is efficient in different wavelengths. In addition, quantum efficiency (QE) of samples **A** and **C** were determined by various monochromatic lights with different band-pass filters (λ = 700, 800 and 900 nm) and results are shown in table S3. Relatively high QE was achieved in long-wavelength region owing to SPR effect of Cu NPs and assistance of CQDs.

Photocatalytic H_2 evolution of physical mixture between Cu and CQDs was performed and results are shown in Fig. S8. The rate of H_2 evolution from the reaction solution for first hour is a bit slow, presumably due to the time it takes for the Cu NPs to form. From the second to the first ten hours, hydrogen evolution of physical mixture Cu and CQDs is similar to pure Cu NPs. No significant improvement of hydrogen evolution is obtained after 5 h with presence of CQDs, indicating that there is no efficient contact between Cu and CQDs with physical mixture. In contrast, efficient contact in sample **C** between Cu and CQDs was proved indirectly which has an evident enhancement of photocatalytic hydrogen evolution.

3.3. Mechanism

The transient photocurrent tests of samples were evaluated via several on/off cycles of irradiation as shown in Fig. 6a. All samples are prompt in generating transient photocurrent during repeated on/off cycles and there is no photocurrent response under dark conditions. The photocurrent value rapidly increases to a constant as soon as light is turned on, and then decrease to zero when light is turned off, exhibiting good repeatability. Apparently, sample **C** shows the highest value than others and this result is consistent with hydrogen evolution rate. Meanwhile, the lowest value of sample **A** also confirms that separation and transportation of photogenerated electron-hole pairs can be enhanced by CQDs. Lifetime of the photoinduced electron could be prolonged

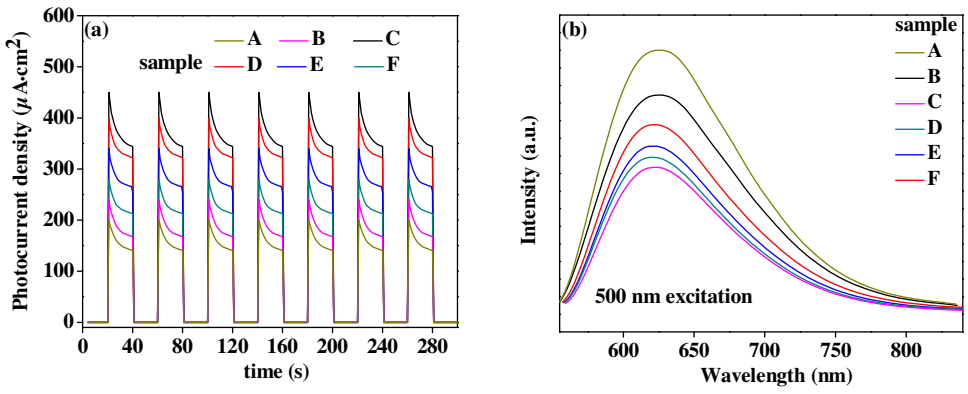

Fig. 6. (a) Photocurrent response under solar light irradiation and (b) photo-luminescence spectra for samples **A**–**F**.

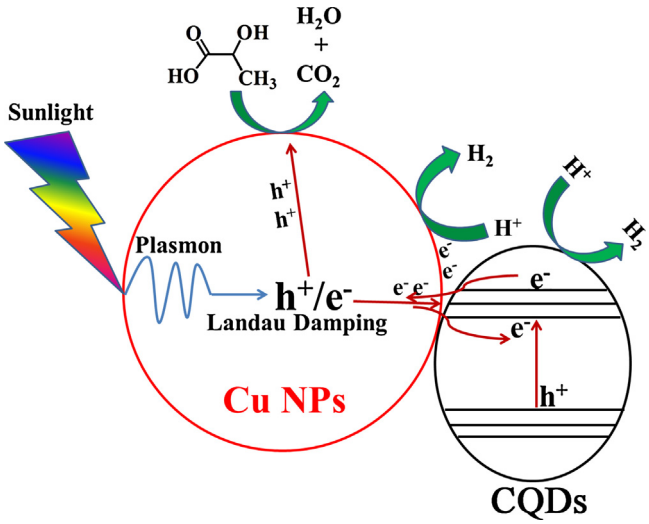

Fig. 7. Schematic of photocatalytic hydrogen evolution over the Cu/CQDs system.

effectively rather than rapid recombination. This great rise in the photocurrent output leads to efficient separation of photo-excited electron-hole pairs, which consequently may be beneficial to photocatalytic hydrogen evolution [46].

To acquire the further insight about the interaction between CQDs and Cu NPs, photo-luminescence (PL) spectroscopy of Cu/CQDs and Cu NPs were carried out as shown in Fig. 6b. Strong emission peaks are assigned to the recombination of the electron-holes which can be prevented by introducing CQDs combined with Cu NPs. Sample **A** shows the highest value and decreases with presence of CQDs, revealing that recombination of photogenerated electron-hole pair is inhibited in the Cu/CQDs due to existence of electron collectors (CQDs). PL intensity of sample **C** is the smallest indicating that it is the optimal content to suppress recombination which is consistent with the tendency of photocatalytic H_2 rate. As the content of CQDs increases continuously, Cu/CQDs nanocomposites aggregate into large particles and become recombination centers to decrease suppression [47]. With the decrease of recombination of photogenerated charge carriers, more electrons will participate in photocatalytic reaction which is mainly influenced by the effective separation and transportation of electron-hole pair [48]. The corresponding photo-excited electron lifetime of samples was also investigated by time resolved fluorescence spectra and results are shown in table S4. An evident decrease of lifetime for Cu/CQDs is observed. This phenomenon proves that dynamic photo-luminescence quenching in the Cu/CQDs system is ascribed to an ultrafast electron transfer process from Cu NPs to CQDs in the system [49]. Furthermore, photocurrent-potential curves, EIS Nyquist plots and photoluminescence spectra of 2-hydroxyterephthalic acid formed by the reaction of terephthalic acid with •OH radicals generated under solar light irradiation of samples were also investigated to illustrate electron transfer properties and results are shown in Fig. S9.

Based on the above results and discussions, the reaction mechanism diagram of Cu/CQDs is proposed in Fig. 7. Cu NPs were formed by photoreduction in lactic acid solution with copper acetate as precursor [9]. Cu NPs are excited by incident light and the collective oscillation of resonant photon-induced electrons will happen which decay into single electron-hole pair excitations through Landau damping [50]. Schematic diagram of collective oscillation of resonant photon-induced electrons is shown in Fig. S10. With the adding of CQDs, photogenerated electrons can be shuttled freely to the conducting texture of CQDs and accepted from Cu NPs due to their excellent electronic conductivity and large electron-storage capacity [14–16], promoting effective separation of photogenerated electron-hole pair, which is also proved by PL measurement, transient photocurrent response, photocurrent-potential curves, EIS Nyquist plots and photoluminescence spectra of 2-hydroxyterephthalic acid formed by the reaction of terephthalic acid with •OH radicals generated under solar light irradiation. Accumulation of electrons will be obtained on the CQDs and then combined with H^+ on the surface of CQDs to form H_2 [51,52]. Meanwhile, the photogenerated holes on Cu NPs could participate in the photocatalytic oxidation reaction with lactic acid [53]. In this process, CQDs act as an electron reservoir to trap electrons generated from Cu NPs and hinder electron-hole pair recombination. As a result, the introduction of CQDs greatly improved the photocatalytic activity because photocatalytic activities are mainly influenced by the effective separation of electron-hole pairs.

4. Conclusions

In summary, Cu/CQDs photocatalysts were designed and prepared *in-situ*. The novel nanocomposites performed enhanced photocatalytic ability for hydrogen evolution under sunlight irradiation compared with pure Cu NPs. CQDs act as an electron reservoir to trap electrons generated from Cu NPs and hinder electron-hole pair recombination. In addition to achieving the highest activity of Cu/CQDs photocatalyst, we demonstrated that Cu/CQDs photocatalyst sustained activity after six recycling tests. Long-wavelength (700, 800 and 900 nm) light photacatalytic properties of photocatalysts were also investigated and they still keep photacatalytic activities for H_2 evolution. Moreover, the photocatalytic hydrogen mechanism was illustrated via the measurements of PL, transient photocurrent, photocurrent-potential curves, EIS Nyquist plots and so on. This work may be significant to provide a new approach to develop a novel catalyst design towards environmental issues, green chemistry and new energy sources.

Acknowledgements

We are grateful to the National Natural Science Foundation of China (No. 21571064, 21371060) and the Fundamental Research Funds for the Central Universities (No. 2015ZM162). We thank Benjamin J. Deibert for proofreading this article.

Appendix A. Supplementary data

Supplementary data associated with this article can be found, in the online version, at http://dx.doi.org/10.1016/j.apcatb.2017.01.051.

References

[1] T. Hisatomi, J. Kubota, K. Domen, Chem. Soc. Rev. 43 (2014) 7520–7535.
[2] X. Zhou, G. Liu, J. Yu, W. Fan, J. Mater. Chem. 22 (2012) 21337–21354.
[3] S. Linic, P. Christopher, D.B. Ingram, Nat. Mater. 10 (2011) 911–921.
[4] C. Clavero, Nat. Photonics 8 (2014) 95–103.
[5] J. Li, S.K. Cushing, F. Meng, T.R. Senty, A.D. Bristow, N. Wu, Nat. Photonics 9 (2015) 601–607.
[6] M.J. Kale, T. Avanesian, P. Christopher, ACS Catal. 4 (2014) 116–128.
[7] P. Christopher, H. Xin, A. Marimuth, S. Linic, Nat. Mater. 11 (2012) 1044–1050.
[8] F. Dong, T. Xiong, Y. Sun, Z. Zhao, Y. Zhou, X. Feng, Chem. Commun. 50 (2014) 10386–10389.
[9] H. Liu, T. Wang, H. Zeng, Part. Part. Syst. Char. 32 (2015) 869–873.
[10] J. Huo, H. Zeng, J. Mater. Chem. A 3 (2015) 17201–17208.
[11] J. Huo, H. Zeng, Appl. Catal. B: Environ. 199 (2016) 342–349.
[12] Y. Xing, J. Wang, L. Chen, J. Mater. Sci-Mater. Electron. 8 (2016) 8633–8640.
[13] S. Xu, J. Ng, X. Zhang, H. Bai, D.D. Sun, Int. J. Hydrog. Energy 35 (2010) 5254–5261.
[14] X. Li, H. Wang, Y. Shimizu, A. Pyatenko, K. Kawaguchi, N. Koshizaki, Chem. Commun. 47 (2011) 932–934.
[15] S.Y. Lim, W. Shen, Z. Gao, Chem. Soc. Rev. 44 (2015) 362–381.
[16] X. Yu, J. Liu, Y. Yu, S. Zuo, B. Li, Carbon 68 (2014) 718–724.

[17] J. Di, J. Xia, Y. Huang, M. Ji, W. Fan, Z. Chen, H. Li, Chem. Eng. J. 302 (2016) 334–343.
[18] W. Shi, X. Zhang, J. Brillet, D. Huang, M. Li, M. Wang, Y. Shen, Carbon 105 (2016) 387–393.
[19] J. Liu, Y. Liu, N. Liu, Y. Han, X. Zhang, H. Huang, Science 347 (2015) 970–974.
[20] K. Li, F.Y. Su, W.D. Zhang, Appl. Surf. Sci. 353 (2016) 110–117.
[21] X. Qian, D. Yue, Z. Tian, Appl. Catal. B: Environ. 193 (2016) 16–21.
[22] J. Liu, W. Zhu, S. Yu, X. Yan, Carbon 79 (2016) 369–379.
[23] J. Tian, Y. Leng, Z. Zhao, Y. Xia, Y. Sang, P. Hao, Nano Energy 11 (2015) 419–427.
[24] Y. Zhang, M. Park, H.Y. Kim, M. El-Newehy, K.Y. Rhee, S.J. Park, Compos. Part B 80 (2015) 355–360.
[25] J. Huo, H. Zeng, J. Mater. Chem. A 3 (2015) 6258–6264.
[26] J. Huo, L. Fang, Y. Lei, G. Zeng, H. Zeng, J. Mater. Chem. A 2 (2014) 11040–11044.
[27] Y. Zhang, M. Park, H.Y. Kim, B. Ding, S.J. Park, Appl. Surf. Sci. 384 (2016) 192–199.
[28] Y. Zhang, M. Park, H.Y. Kim, S.J. Park, J. Alloy Compd. 686 (2016) 106–114.
[29] J. Qin, J. Huo, P. Zhang, J. Zeng, T. Wang, H. Zeng, Nanoscale 8 (2016) 2249–2259.
[30] X. Jin, X. Sun, G. Chen, L. Ding, Y. Li, Z. Liu, Carbon 81 (2015) 388–395.
[31] D. Tang, H. Zhang, H. Huang, R. Liu, Y. Han, Y. Liu, Dalton Trans. 42 (2013) 6285–6289.
[32] C. Wang, Z. Xu, H. Cheng, H. Lin, M.G. Humphrey, C. Zhang, Carbon 82 (2015) 87–95.
[33] H. Li, Z. Kang, Y. Liu, S.-T. Lee, J. Mater. Chem. 22 (2012) 24230–24253.
[34] X. Li, S. Zhang, S.A. Kulinich, Y. Liu, H. Zeng, Sci. Rep. 4 (2014) 4976.
[35] H. Ming, Z. Ma, Y. Liu, K. Pan, H. Yu, F. Wang, Dalton Trans. 41 (2012) 9526–9531.
[36] E.Z. Liu, L.M. Kang, Y.H. Yang, T. Sun, X.Y. Hu, C.J. Zhu, Nanotechnology 25 (2014) 165401.
[37] X. Teng, C. Ma, C. Ge, M. Yan, J. Yang, Y. Zhang, J. Mater. Chem. B 2 (2014) 4631–4639.
[38] S. Liu, J. Tian, L. Wang, Y. Zhang, X. Qin, Y. Luo, Adv. Mater. 24 (2012) 2037–2041.
[39] P. Zhang, T. Wang, H. Zeng, Appl. Surf. Sci. 391 (2017) 404–414.
[40] J.G. Yu, H.G. Yu, B. Cheng, X.J. Zhao, J.C. Yu, J. Phys. Chem. B 107 (2003) 13871–13879.
[41] B.C.M. Martindale, G.A.M. Hutton, C.A. Caputo, E. Reisner, J. Am. Chem. Soc. 137 (2015) 6018–6025.
[42] R. Bashiri, N.M. Mohamed, C.F. Kait, S. Sufian, Int. J. Hydrog. Energy 40 (2015) 6021–6037.
[43] Y. Hou, Q. Lu, H. Wang, Mater. Lett. 173 (2016) 13–17.
[44] X. Xu, G. Liu, C. Randorn, J.T.S. Irvine, Int. J. Hydrog. Energy 36 (2011) 13501–13507.
[45] L. Ge, C. Han, J. Liu, Appl. Catal. B: Environ. 108–109 (2011) 100–107.
[46] J. Di, J. Xia, S. Yin, H. Xu, L. Xu, Y. Xu, RSC Adv. 4 (2014) 14281–14290.
[47] S. Shen, P. Guo, L. Zhao, Y. Du, L. Guo, J. Solid State Chem. 184 (2011) 2250–2256.
[48] M.V. Dozzi, A. Saccomanni, M. Altomare, E. Selli, Photochem. Photobiol. Sci. 12 (2013) 595–601.
[49] R. Liu, H. Huang, H. Li, Y. Liu, J. Zhong, Y. Li, ACS Catal. 4 (2014) 328–336.
[50] H. Petek, S. Ogawa, Prog. Surf. Sci. 56 (1997) 239–310.
[51] Q. Liu, T. Chen, Y. Guo, Z. Zhang, X. Fang, Appl. Catal. B: Environ. 193 (2016) 248–258.
[52] H. Yu, Y. Zhao, C. Zhou, L. Shang, Y. Peng, Y. Cao, L. Wu, C. Tung, T. Zhang, J. Mater. Chem. A 2 (2014) 3344–3351.
[53] J. Chen, X.J. Wu, L. Yin, B. Li, X. Hong, Z. Fan, Angew. Chem. Int. Ed. 54 (2015) 1210–1214.